Master's thesis

NTNU
Norwegian University of Science and Technology
Faculty of Engineering
Department of Energy and Process Engineering

Kris Gabriel and Nora Hundseid

Experimental investigation of the interaction between two roof-mounted Savonius wind turbines

Master's thesis in Mechanical Engineering
Supervisor: Tania Bracchi
June 2023

NTNU
Norwegian University of
Science and Technology

Kris Gabriel and Nora Hundseid

Experimental investigation of the interaction between two roof-mounted Savonius wind turbines

Master's thesis in Mechanical Engineering
Supervisor: Tania Bracchi
June 2023

Norwegian University of Science and Technology
Faculty of Engineering
Department of Energy and Process Engineering

NTNU
Norwegian University of
Science and Technology

Acknowledgements

The authors express their sincere appreciation to their supervisor, Tania Bracchi, for designing an exciting project for the Master's thesis and providing the opportunity to conduct experiments in the wind tunnel at NTNU. The authors are grateful for her valuable contributions to the discussion of the results, as well as for her continuous support and encouragement throughout the duration of this study. The authors extend their sincere gratitude to Girish Kumarsing Jankee and Srikar Yadala for their assistance in conducting particle image velocimetry and for sharing their knowledge about the methodology. The authors would also like to thank Leon Li for his assistance in conducting particle image velocimetry. The authors express their appreciation to Jason R. Hearst for his expertise and valuable contributions to the discussion of the final results. Finally, we would also like to thank Fredrik Fløttum for machining the model building, and Øyvind Haave for constructing the mount for the acrylic plate in the wind tunnel.

Kris Gabriel wishes to show his immense appreciation for his parents and sister for their endless support and sacrifices. Making you proud has been my greatest motivation throughout this journey, and will continue to be so in my next endeavors. To my friends in Lørenskog, and the ones I have been lucky to meet in Trondheim; I will forever cherish the wonderful memories and the nights we may have forgotten. I am confident that our future holds even more remarkable experiences together.

Nora Hundseid expresses gratitude for the fellow master's students at the Waterpower Laboratory who have contributed to making the final year of our studies truly memorable. I would like to extend a special appreciation to Jørgen, for his continuous support as my boyfriend, study partner and friend throughout my years at NTNU.

Preface

This Master's thesis was authored at the Fluid Mechanics Laboratory at the Department of Energy and Process Engineering (EPT) at the Norwegian University of Science and Technology (NTNU) during the spring semester of 2023, under the supervision of Tania Bracchi. The thesis is presented in the form of a research article, aiming to closely resemble a completed publication. The main document is followed by appendices that contain supplementary information not included in the research article but deemed relevant to the Master's thesis.

Problem Description

This study represents an experimental exploration of the interaction between parallel roof-mounted Savonius turbines. While the Savonius turbine has been extensively studied, the investigation of the coupling effect between two ground-mounted Savonius turbines has been limited primarily to numerical analysis. Consequently, there is a significant research gap that necessitates further experimental investigations in this area. The current study serves as a continuation of an ongoing research campaign at NTNU focused on Urban Wind Power. Specifically, the study aims to investigate the previously observed power-enhancing effect in ground-mounted turbines and explore its applicability to roof-mounted turbines. The experiment varied the rotational direction and gap distance of the turbines to investigate their influence on performance. The primary objectives of this project are as follows:

- Design and build the model building
- Acquire power curves for all configurations
- Measure the flow field with planar PIV for all configurations
- Analyze and conclude the results from the experiment

Abstract

This study presents an examination of the interaction between two roof-mounted Savonius turbines parallel to the crossflow. A wind tunnel experiment was conducted to analyze the turbines' power production in relation to their rotational direction and the gap distance between them, resulting in 12 configurations. Power curves were acquired for all configurations and particle image velocimetry (PIV) was employed to visualize the flow field. The results revealed that higher tip-speed ratios led to power enhancement in all configurations compared to a single turbine, indicating a coupling effect between the turbine pair. Conversely, lower tip-speed ratios showed no power enhancement, suggesting a minimum tip-speed ratio requirement for power enhancement. The study also demonstrated that the turbines' overall performance was influenced by their relative rotational direction and the gap distance between them, consistent with previous research on ground-mounted Savonius turbines. The optimal configuration was identified as counter-rotating turbines with advancing buckets positioned in the turbine gap and with a gap distance of 0.4 turbine diameters, resulting in a 24.1% increase in average power coefficient compared to a single roof-mounted turbine. Differences in power enhancement between the left and right turbines were observed for symmetrical rotational cases, attributed to slight variations in circuit resistance and tip-speed ratios. Analysis of the flow field indicated a potential relationship between upstream velocities and turbine performance, while downstream vorticity flow field examination revealed the significant influence of the recirculation region above the roof on wake characteristics. The suppression of vortices in the wake explains the unexpected results in case C and the power enhancement in case B. The findings reveal similarities and differences between ground-mounted and roof-mounted turbines and suggest the need for further investigation into downstream vortices for both cases.

Sammendrag

I denne studien utforskes kraftytelsen og samspillet mellom to parallelt plasserte Savonius-turbiner på en bygning. Eksperimenter ble utført i en vindtunnel med formål om å analysere turbinenes kraftproduksjon ved ulike rotasjonsretninger og avstander mellom turbinene. Totalt ble det undersøkt 12 forskjellige konfigurasjoner. For hver konfigurasjon ble det registrert kraftkurver, og strømningsfeltet ble visualisert ved hjelp av metoden Particle Image Velocimetry (PIV). Resultatene avdekket at høyere tip speed ratio førte til en økning i ytelsen for alle konfigurasjoner sammenlignet med en enkelt turbin, noe som indikerer en koblingseffekt mellom turbinparet. Derimot viste resultatene ingen forbedring i ytelsen når turbinene opererte på lavere tip speed ratio, noe som tyder på at det er en minimum rotasjonshastighet som kreves for at kraftforbedringen skal inntreffe. Studien viser også at den totale ytelsen ble påvirket av den relative rotasjonsretningen og avstanden mellom turbinene, noe som er i samsvar med tidligere studier av Savonius-turbiner på bakken. Den optimale konfigurasjonen ble funnet å være når turbinene roterer i motsatt retning med fremskytende skovler plassert i gapet mellom de to rotorene, med en turbinavstand på 0.4 turbindiametere. Turbinene i denne konfigurasjonen oppnådde en gjennomsnittlig økning i kraftkoeffisient på 24.1% sammenlignet med en enkeltstående turbin på samme bygning. Det ble observert en forskjell i kraftforbedring mellom høyre og venstre turbin i tilfeller med symmetrisk rotasjon som skyldes små variasjoner i kretsresistans og tip speed ratio. Analyser av hastighetsfeltet avdekket en mulig sammenheng mellom oppstrøms hastigheter og turbinytelse, mens analyser av virvelfeltet nedstrøms viste at resiskulasjonsområdet over bygningen hadde betydelig innvirkning på vakeegenskapene til turbinene. Undertrykkelse av virvler i vaken kan forklare det uventede resultatet for case C og kraftforbedringen for case B. Funnene avdekket likheter og forskjeller mellom bygningsturbiner og bakkemonterte turbiner og indikerer et behov for videre undersøkelser av nedstrømsvirvler for begge tilfeller.

Contents

Experimental investigation of the interaction between two roof-mounted Savonius wind turbines

Kris Gabriel and Nora Hundseid

Abstract

This study presents an examination of the interaction between two roof-mounted Savonius turbines parallel to the crossflow. A wind tunnel experiment was conducted to analyze the turbines' power production in relation to their rotational direction and the gap distance between them, resulting in 12 configurations. Power curves were acquired for all configurations and particle image velocimetry (PIV) was employed to visualize the flow field. The results revealed that higher tip-speed ratios led to power enhancement in all configurations compared to a single turbine, indicating a coupling effect between the turbine pair. Conversely, lower tip-speed ratios showed no power enhancement, suggesting a minimum tip-speed ratio requirement for power enhancement. The study also demonstrated that the turbines' overall performance was influenced by their relative rotational direction and the gap distance between them, consistent with previous research on ground-mounted Savonius turbines. The optimal configuration was identified as counter-rotating turbines with advancing buckets positioned in the turbine gap and with a gap distance of 0.4 turbine diameters, resulting in a 24.1% increase in average power coefficient compared to a single roof-mounted turbine. Differences in power enhancement between the left and right turbines were observed for symmetrical rotational cases, attributed to slight variations in circuit resistance and tip-speed ratios. Analysis of the flow field indicated a potential relationship between upstream velocities and turbine performance, while downstream vorticity flow field examination revealed the significant influence of the recirculation region above the roof on wake characteristics. The suppression of vortices in the wake explains the unexpected results in case C and the power enhancement in case B. The findings reveal similarities and differences between ground-mounted and roof-mounted turbines and suggest the need for further investigation into downstream vortices for both cases.

1. Introduction

The world's growing population and increasing energy demand (Roser et al., 2013) have highlighted the need for renewable energy sources to mitigate climate change. Wind energy, as a globally abundant resource, has experienced steady growth over the past decade and is a leading non-hydro renewable energy technology (International Energy Agency, 2022). While large-scale wind farms have dominated global wind energy production, there is a rising interest in on-site power generation, particularly in urban areas. Roof-mounted wind turbines have emerged as a potential solution for local renewable energy production in urban areas, complementing solar power systems. These turbines capitalize on available wind resources, reduce grid maintenance, and minimize transmission losses. Although solar power has been widely adopted for on-site generation, advances in roof-mounted wind turbines offer opportunities for urban wind power and address the challenges

of wind resource availability and building design. As a result, integrating wind turbines into urban environments can contribute to the local production of renewable energy while enhancing sustainability and reducing dependence on traditional power grids.

Optimizing the power production per unit land is important in urban areas where space is limited. There are two types of turbines; horizontal axis wind turbines (HAWT) and vertical axis wind turbines (VAWT). The power density of a horizontal axis and vertical axis wind turbine farm were compared in a study by Dabiri (2011). When VAWTs are arranged in layouts that enable them to extract energy from adjacent wakes, the power density is an order of magnitude higher than the HAWT farm. In addition, VAWTs are better suited for an urban environment since they are less susceptible to gusts and changes in wind direction, leading to less maintenance than HAWTs (Pagnini et al., 2015). Mertens (2003) investigated the energy potential of VAWTs installed on flat roof buildings. Emphasis was placed on the significance of the recirculation bubble that forms on top of the roof due to flow separation at the windward top edge, in which the flow is highly turbulent and backflow occurs. As a result, the mean flow experiences a skew angle that varies along the roof, accompanied by an accelerated flow region on top of the recirculation bubble. A similar recirculation bubble will also form on top of a rib (Shah et al., 2009). The influence of turbine position on the building and turbine height was investigated in a study by Jooss et al. (2022b) using a small-scale Savonius turbine. The turbine positioned at a greater height above the roof outperformed the turbine positioned closer to the roof because the taller turbines effectively harnessed the increased momentum of the airflow on top of the recirculation area. This led to higher power output and reduced dependency on the position of the turbine on the roof. In conclusion, the study demonstrates that the presence of a model building significantly enhances the performance of the roof-mounted wind turbine compared to the turbine operating on the ground.

Roof-mounted turbines show increased performance when they are placed in the accelerated flow region above the recirculation area, however, there are several ways to increase the performance of a Savonius wind turbine. The first option is geometry optimization of the rotor design such as blade shape, blade overlap, and gap. Methods to reduce the anti-rotation torque of the rotor shaft have also been studied and involves adding extra objects, such as a duct to redirect the flow in a favorable manner (Xiaojing et al., 2012). Another way of increasing the performance of a Savonius wind turbine is to arrange them in clusters of two or more turbines. Studies have investigated the interaction between two Savonius turbines installed next to each other on a flat plate, and they have reported enhanced power output compared to a single turbine (Hesami et al., 2022; Jang et al., 2016; Laws, 2022; Shaheen et al., 2015; Shigetomi et al., 2011; Xiaojing et al., 2012). The turbines experience enhanced power production due to the periodic coupling of flow between the turbines, which is associated with vortex shedding and cyclic pressure fluctuations (Shigetomi et al., 2011). The enhancement is dependent on the gap distance, the rotational direction and the relative phase angle between the two turbines, and the coupling effect has a greater influence on the Savonius turbines at close gap distances (Xiaojing et al., 2012).

Xiaojing et al. (2012) performed a numerical study of the coupling effect between two Savonius turbines. Their numerical results reveals that the gap distance and relative phase angle have a significant influence on the positive interaction between the turbines. The highest power coefficient is achieved when the rotors counter-rotate, with the advancing blades positioned in the gap between the rotors. This configuration, with a relative phase angle of 90° and a gap distance of 0.2D-0.4D, resulted in the most favorable performance. The performance is drastically lowered for other relative phase angles, which perform better for larger gap distances. When the turbines counter-rotates in the opposite direction, the relative angle have less impact and no significant power enhancement

is observed. In the case of two turbines co-rotating in the same direction, an enhanced average power coefficient is observed at reduced gap distances, and the relative phase angle does not have a significant effect. Shaheen et al. (2015) did a numerical investigation on the performance of multiple Savonius turbines in a cluster. As part of their study, they examined two Savonius turbines placed in parallel and found that both turbines performed optimally at a gap distance of 0.2D. Their investigation focused on co-rotating turbines, with a constant relative phase angle of 0 degrees. They did not consider other relative phase angles. The turbines performed significantly worse for a gap distance of 0.1D, which was the smallest gap distance they investigated. Two turbines in parallel were studied in order to find the optimal gap distance before investigating a cluster of three oblique turbines. Hesami et al. (2022) performed a numerical study on one and two Savonius turbines with a wind-lens. Their study concluded that a gap distance of $0.45D$ (the smallest distance tested) resulted in a 114% increase in the maximum power coefficient $C_{p,max}$ compared to a single open turbine. This performance enhancement was observed when the turbines counter-rotated and the advancing blades were positioned in the gap between the turbines. Hesami et al. (2022) did not specify the relative phase angle used in their study. Laws (2022) conducted a numerical investigation on the coupling effect between two Savonius turbines with modified blades using free rotation analysis. They examined both co-rotating and counter-rotating turbine configurations and found that the best performance was achieved by co-rotating turbines at a gap distance of 0.2D, which was the smallest distance tested. The performance of the co-rotating turbines decreased as the gap distance increased. Jang et al. (2016) did an experimental study on doublet Savonius turbines to explore the effect of gap distance. They test the gap distances 1.0D and 1.5D, along with three rotational directions. Their findings indicate that the turbines perform best when co-rotating in the same direction with a gap distance of 1.5D. When the turbines counter-rotate with the advancing buckets positioned in the gap between them, the overall performance is worse. However, it is worth noting that for this specific configuration, the turbines exhibit improved performance when the gap distance is set at 1.0D instead of 1.5D. It's important to note that the experimental results of Jang et al. (2016) differ significantly from the findings of previous numerical studies (Hesami et al., 2022; Shaheen et al., 2015; Xiaojing et al., 2012). Jang et al. (2016) did not discuss or specify the control of the relative phase angle between the two turbines, which could potentially offer a plausible explanation for the discrepancy.

In this section, we previously discussed the benefits and potential of roof-mounted turbines compared to ground-mounted ones, which is mainly due to the accelerated flow region above the recirculation bubble that forms on top of buildings. Several studies have explored the impact of gap distance and rotational direction on the performance of ground-mounted turbines. However, the interaction between roof-mounted turbines placed parallel to the cross-flow remains unexplored. This research gap has motivated the present study, which aims to address the following research question: How does the interaction between two roof-mounted Savonius turbines affect their performances? Consequently, the research objectives of this study include examining the performance of the two roof-mounted turbines at different gap distances and rotational directions, with the aim of identifying the optimal configuration for maximizing power production. Specifically, the relative gap distances were set at [0.1, 0.2, 0.4, 0.8], and three combinations of rotational directions were considered to encompass both co-rotating and counter-rotating turbine configurations. The control of the relative phase angle between the turbines was not incorporated in this experiment due to the requirement for advanced regulation systems. As a result, the scope of this project does not encompass the control of the relative phase angle. Nevertheless, a concise discussion on the relative phase angle is included in the results section of the present study. Additional research objectives

include acquiring the flow field data for all turbine configurations and utilizing it to explain the effects and phenomena contributing to the observed turbine performance. To achieve these research objectives, wind tunnel experiments were conducted on small-scale Savonius turbines. These turbines were positioned close to the leading edge of a square rib. A rib was chosen as a model building in order to be independent of the ratio between turbine diameter and building width, as this ratio can vary greatly in urban areas. The turbine performance was assessed by measuring the C_p-curves, while flow field measurements were obtained using particle image velocimetry (PIV). It is worth mentioning that the scope of the project did not include optimizing the turbine design for power production.

2. Experimental Procedure

2.1. Wind tunnel setup

The experiment was conducted in a closed-loop wind tunnel at the Norwegian Institute of Science and Technology and is based on a previous experiment by Jooss et al. (2022b). An illustration of the setup in the wind tunnel is presented in Figure 1 and pictures of the setup is provided in Appendix C. The dimensions of the wind tunnel's test section are 2.71 m×1.80 m×11.15 m (width×height×length). A rectangular acrylic plate was used to model the ground and was mounted 1 m above the wind tunnel floor on aluminum legs to avoid the boundary layer that occurs on the floor. The dimensions of the plate are 1.8 m × 3 m × 0.01 m (width×length×thickness). The leading edge of the plate has a 15° angle to prevent flow separation and a roughness strip is placed downstream of the leading edge to trip the boundary layer and ensure that the boundary layer transitions at the same position for all measurements. The freestream velocity between the plate and the wind tunnel floor was set to $U_\infty = 9.05\ m/s \pm 0.5\ m/s$, and was measured with a pitot-static tube. Additionally, the temperature and atmospheric pressure were measured with a K-type thermocouple and a mercury barometer, respectively.

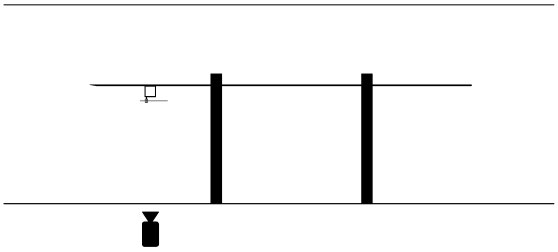

Figure 1: Side-view sketch of the wind tunnel setup. The wind travels from left to right.

To avoid the spanwise effect caused by the edges on the sides of a building, a square aluminum rib was selected as the model building. Thus, the flow above the rib only varied in the vertical and downstream directions. Figure 2 illustrate the components used in the wind tunnel. Here, $h = 100mm$ is defined as the height of the rib. The rib was mounted $5h$ from the leading edge of the acrylic plate and on the underside of the plate as this was more convenient when considering the PIV setup, which will be described in Section 2.4. The rib dimensions are 1.80 m×0.1 m×0.1 m (width×length×height). The surface was milled to ensure a sharp edge since the flow behaviour is highly dependent on the shape of the building edge (Toja-Silva et al., 2015). The Reynolds number

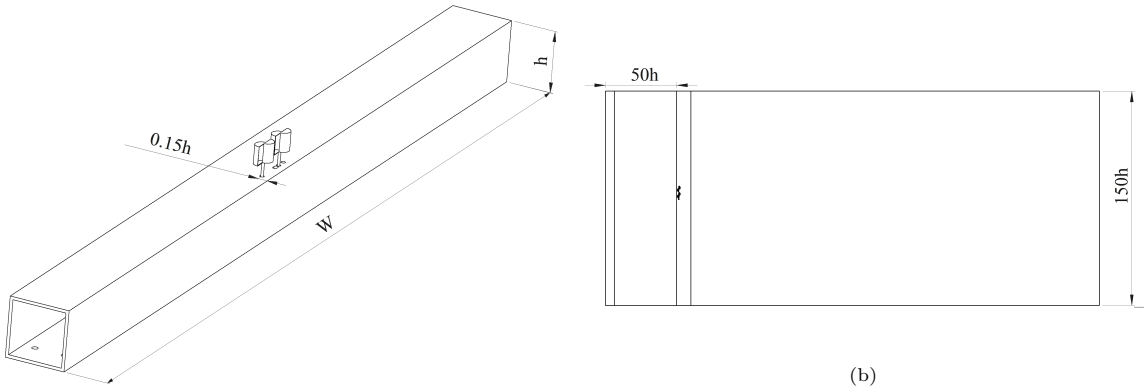

(a) (b)

Figure 2: Sketch of rib and plate with dimentions. (a) shows the position of the turbines on the model building, (b) displays the position of the model building on the plate.

based on the height of the rib, h, was $Re_h \approx 60\,000$. Five mounting holes were drilled $0.15h$ from the leading edge on top of the rib so that the turbines could be mounted in multiple positions. To investigate the influence of the gap distance, S, between a turbine pair, four gap distances were examined. S is defined in Figure 4 together with turbine 1 (T1) and turbine 2 (T2). The relative gap distances S/D are 0.1. 0.2, 0.4 and 0.8, and will hereafter be denoted as P1, P2, P3 and P4.

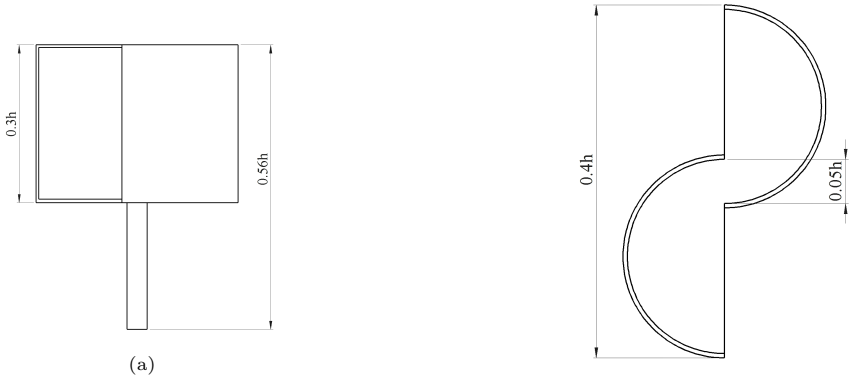

(a) (b)

Figure 3: Sketch of turbine with dimensions . (a) displays the profile of the Savonius VAWT and (b) shows the cross section of the Savonius turbine. Turbine design by Jooss et al. (2022a).

A two-bucket Savonious wind turbine with overlapping buckets and end plates was used in the experiment and is identical to the turbine used in Jooss et al. (2022b). The turbine is illustrated in Figure 3. The rotor diameter d_t is $0.4h$, resulting in a Reynolds number, $Re_{d_t} \approx 24\,000$. The turbine has a shaft diameter of $0.04h$ and was mounted such that the bottom of the turbine buckets was $h_t = 0.16h$ above the roof of the model building. An Ultimaker S5 3D printer was used to produce the turbine in polylactide (PLA). It is worth mentioning that the scope of this project did

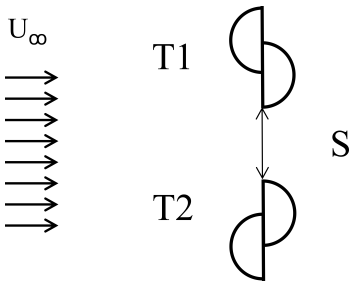

Figure 4: Definition of gap distance (S), left turbine (T1) and right turbine (T2) when looking downstream.

not include optimizing the turbine design for power production. To explore the effect of turbine rotational direction on power generation, two turbines were produced. More specifically, a clockwise turbine and a counter-clockwise turbine were designed, representing the rotational scenarios in Figure 5. The parallel turbine pair in cases A and B are counter-rotating, while case C is co-rotating clockwise. Case A is rotating with the advancing buckets positioned in the gap between the turbines and case B is rotating with the returning buckets positioned in the gap between the turbines. Hereafter, rotational case A in position 1 will be referred to as A1, and similarly for the other combinations of configurations.

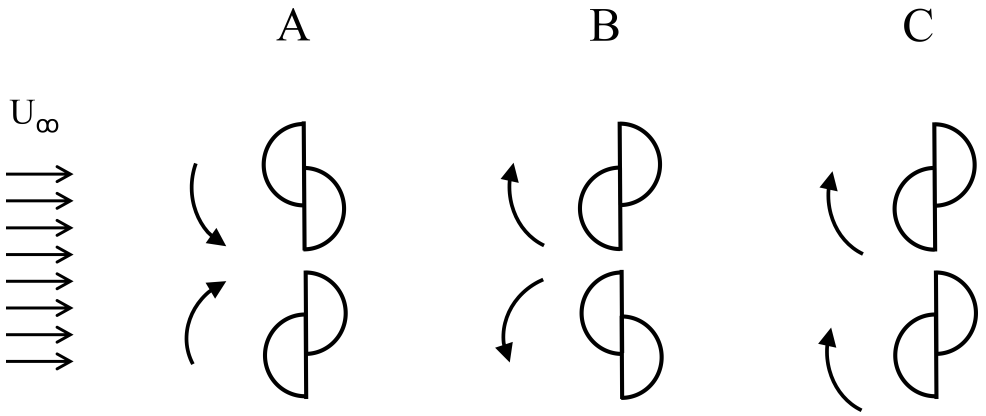

Figure 5: Definition of rotational cases A, B, C and D.

2.2. Power acquisition

The combination of gap distances and rotational cases resulted in 12 different configurations, in addition to a reference case which consisted of a single turbine on the rib. To understand how and to what degree the turbines influence each other in the different configurations it is crucial to measure the power produced by both turbines in each configuration. The method for acquiring the power produced is based on a previous study conducted by (Jooss et al., 2022b). The mechanical power, P_m, is calculated as $P_m = P_c - P_f$, where P_c is the converted power from the wind and P_f is the friction losses. P_f is calculated as the product between the estimated torque friction, Q_f, and the rotational velocity of the turbine, ω. The turbines were coupled to brushed DC motors

(12G88 Athlonix) to produce electrical power, thus, the mechanical power is found by $P_m = Q_{em}\omega$ where Q_{em} is the electromagnetic torque of the motors. A reflective tape was placed on half the circumference of the bottom end of the turbine shafts, and a reflective object sensor (OPB705WZ) was used to acquire the turbine's rotational velocity at a frequency of approximately 300 Hz and a sampling time of 120 seconds. The rotational velocity did not exceed 62 Hz, thus the sampling rate was sufficient according to the Nyquist–Shannon sampling theorem (Shannon, 1949). Q_{em} was calculated as the product of the motor's torque constant, $K_T = 4.9\, mNm/A$, and the current, I. An INA219 High Side DC Current Sensor was used to measure the produced current over a $0.1\,\Omega$ resistor. To measure the performance of the turbines at different tip-speed ratios, λ, a high-frequency variable switch (IRF540NPbF) was used to vary the effective resistance in the circuit. The adjustable switching frequency is represented by the variable k, which is a value between 0 and 255. For each measurement of C_P, the same k-value was implemented for both turbines. An Arduino UNO was used for the turbine control and the acquisition of ω and I. Further, the coefficient of power, Cp, was calculated for each λ by Equation 1.

$$C_P = \frac{P_m}{\frac{1}{2}\rho A U_\infty^3} \tag{1}$$

Here, ρ is the air density and A denotes the rotor area. The instantaneous free stream velocity U_∞ was measured with the pitot-static tube. The instantaneous density ρ was determined from the ideal gas law, utilizing the instantaneous temperature T measured from a K-type thermocouple. The ideal gas law equation is $\rho = \frac{p_{atm}}{RT}$, with the atmospheric pressure p_{atm} acquired with a mercury barometer and R representing the ideal gas constant. An uncertainty analysis based on Wheeler et al. (2010) yielded a maximum uncertainty for C_P and λ as 2.80% and 1.34%, respectively. The methodology is described in Appendix B.

2.3. Uncertainties in electrical setup

Two turbines, T1 and T2, were used in this experiment. Each turbine was connected to an individual electronic setup consisting of identical components. These setups enabled power measurements to be obtained for each turbine. However, a discrepancy was observed in the C_P-curves when sampling with the different setups despite the components being identical. This discrepancy was due to lower resistance in the circuit for T2 compared to T1 for the same k-value (described in Section 2.2). To examine the impact of this electronic variation, a series of experiments were conducted in an open wind tunnel produced by Gunt Hamburg with a cross-sectional area of $0.292m^2 \times 0.292m^2$. The details of these experiments are described in Appendix A. From the results of the first two experiments, it was concluded that adjusting the power curves of turbine 2 solely based on the difference in resistance would be insufficient, considering the influence of the turbines on each other. Based on the results of the last experiment, it was determined that using the reference curve obtained for T1 is adequate for comparing the power curves of both T1 and T2.

2.4. PIV

The velocity fields around the turbines were obtained to study the correlation between flow phenomena and the performance of the turbines. The velocity fields were acquired using planar particle image velocimetry (PIV) in the horizontal plane. While capturing the images, the turbines were operating at the optimum λ for the respective turbine configuration. The PIV setup is illustrated in Figure 6. The flow is seeded with DHS particles with a diameter of 1 μm. A Litron LDY303HE laser with a wavelength of 527 nm and a maximum pulse energy of 28 mJ serves as the light source to illuminate the particles. The laser pulse frequency is set to 307 Hz, ensuring it satisfies the Nyquist sampling frequency with respect to the turbine's maximum vortex shedding frequency of 120 Hz.

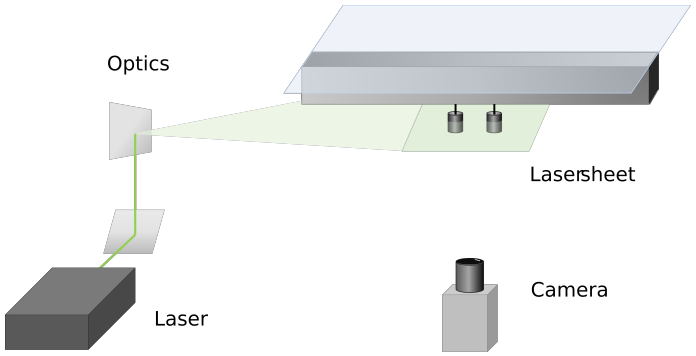

Figure 6: Illustration of PIV-setup.

A Phantom v2012 high-speed camera equipped with a Sigma 180 mm lens is used to capture images of the flow. The camera features a sensor resolution of 1 MP (1280 px $\times$ 800 px) and has a pixel pitch of 28 microns. During image acquisition, an aperture of 5.6 was used and 6200 images were captured, which corresponds to 20 seconds of flow field measurement. This provides a sufficient estimate of the average flow field when the images are post-processed. The camera and lens provided a field of view (FOV) measuring 180 mm $\times$ 250 mm (width $\times$ length). The flow upstream and downstream of the building was split and processed separately due to different velocity and pixel displacement, which was caused by the presence of the recirculating area. The upstream FOV measured 180 mm $\times$ 57 mm and the downstream FOV measured 180 mm $\times$ 143 mm. To ensure accurate visualization of the flow, a mask was applied during the pre-processing stage to prevent any distortions caused by the turbine's shadow and reflection. The software Davis 10 was used to calculate vector fields from the particle images. The vector spacing was 3.58 mm and 3.60 mm in the x- and y-direction, respectively. For the correlation window size, 3 passes at 32 $\times$ 32 pixels with 50% overlap in all passes were used to reduce the in-plane pair loss error. The velocity fields obtained using PIV were used to calculate the vorticity of the flow field downstream of the model building to visualize vortex formation in the turbine wakes. The vorticity is defined in Equation 2(Arendt, 1993), where U is the velocity in the streamwise direction and V is the velocity in the cross-flow direction.

$$\boldsymbol{\omega} = \nabla \times \mathbf{U} = \frac{\partial \mathbf{V}}{\partial x} - \frac{\partial \mathbf{U}}{\partial y} \tag{2}$$

3. Results

3.1. Power Measurements

The power curves for all configurations are illustrated in Figure 7 together with the power curve of the reference case. Figure 7a-7c show the left turbine (T1) and Figure 7d-7f show the right turbine (T2). The error bars denote uncertainties of 2.8% for C_P and 1.34% for λ, as stated in Section 2. The C_p-curves show relatively low values (< 0.08) which can be explained by the low Reynolds number (Akwa et al., 2012; Aliferis et al., 2019) resulting from the use of small-scale turbines in this experiment. The low C_P-values shown by the figures align with the findings reported by Jooss et al. (2022b). The maximum power coefficient for the reference case, consisting of a single roof-mounted turbine, was determined to be $C_{P,ref,max} = 0.058$ at the corresponding optimal tip-speed ratio $\lambda_{ref,opt} = 0.377$. The power curves exhibit no power enhancement for the turbines at low tip speed ratios ($\lambda < 0.2$) as the turbines show no improvement compared to the reference case. This indicates that the turbines do not influence each other at low λ. However, a power-enhancing effect is observed at higher tip speed ratios for all configurations, clearly showing that the turbines influence each other at higher λ. Furthermore, the differing C_P-curves of T1 and T2 for the symmetrical cases (A and B) are considered to be a result of differing λ, as described in Section 2.3.

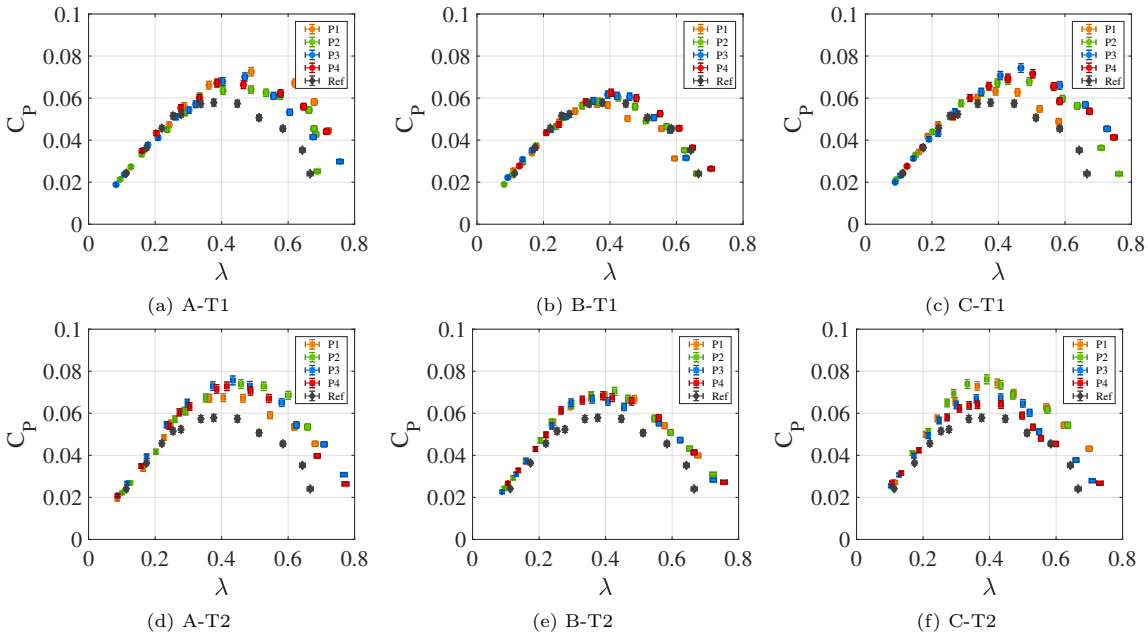

(a) A-T1 (b) B-T1 (c) C-T1

(d) A-T2 (e) B-T2 (f) C-T2

Figure 7: Power curves for each rotational case. Turbine 1: (a)-(c), Turbine 2: (d)-(f).

The relative change in power enhancement is used as a quantitative method to compare the power enhancement for different turbine configurations. The equation is given by $\Delta\overline{C}_{P,max} = \frac{\overline{C}_{P,max} - C_{P,ref,max}}{C_{P,ref,max}}$, where $\overline{C}_{P,max}$ is the maximum average power coefficient of the turbine pair and $C_{P,ref,max}$ is the maximum power coefficient for the reference case. The relative changes in turbine performance parameters are summarized in Table 1. The power enhancement in the far right

column is visually represented using a color scheme of three shades of green, with darker shades indicating a higher degree of power enhancement. As observed in Table 1, all turbine configurations exhibit a positive $\Delta\overline{C}_{P,max}$ which indicates a power enhancement across all configurations when compared to the reference case (single turbine on building). Overall, case A demonstrated the highest performance, followed by case C, while case B exhibited the lowest performance. Moreover, each case will be thoroughly analyzed in the following paragraphs.

Table 1: Summary of wind turbine performance parameters with comparison to reference case for all configurations.

		λ_{opt}		$\Delta C_{P,max}$*		
		T1	T2	T1	T2	$\Delta\overline{C}_{P,max}$†
A	1	0.489	0.464	25.5%	16.0%	20.8%
	2	0.533	0.527	8.1%	25.9%	17.0%
	3	0.403	0.434	17.4%	30.7%	24.1%
	4	0.386	0.487	16.1%	22.0%	19.1%
B	1	0.360	0.355	-1.3%	17.3%	8.0%
	2	0.365	0.427	0.9%	21.7%	11.3%
	3	0.393	0.407	6.7%	13.5%	10.1%
	4	0.404	0.420	8.0%	16.6%	12.3%
C	1	0.391	0.423	9.3%	28.3%	18.8%
	2	0.397	0.434	16.2%	27.2%	21.7%
	3	0.468	0.500	28.4%	11.9%	20.2%
	4	0.428	0.434	20.0%	10.9%	15.5%

$*\Delta C_{P,T1,max} = \frac{C_{P,T1,max} - C_{P,ref,max}}{C_{P,ref,max}}$, $\Delta C_{P,T2,max} = \frac{C_{P,T2,max} - C_{P,ref,max}}{C_{P,ref,max}}$

$\dagger\Delta\overline{C}_{P,max} = \frac{\overline{C}_{P,max} - C_{P,ref,max}}{C_{P,ref,max}}$

The best performance was observed for configuration A3 which exhibited a 24.1% increase in the maximum average power coefficient of the turbine pair. Additionally, case A performed the best across all gap distances, except for $S = 0.2D$ where case C performed better. It is worth mentioning that all cases, particularly case A, exhibited significant power enhancement regardless of the gap distance, indicating a relatively low sensitivity to variations in this parameter. These findings are consistent with the research conducted by Xiaojing et al. (2012) for case A.

It is important to note that the relative phase angle was not actively controlled in this study, as previously mentioned in Section 2.1. Analysis of the particle image velocimetry (PIV) images revealed continuous variations in the relative phase angle throughout the experiment. This variation in the relative phase angle also accounts for the relatively lower power enhancement observed in this present study compared to the results reported by Xiaojing et al. (2012) when considering the optimal relative phase angle of 90°.

Case B showed the lowest average improvement for all gap distances and was the worst rotational configuration. However, power enhancement was still observed compared to a single turbine on a building. Interestingly, no significant power enhancement was observed for ground-mounted turbines in case B (Xiaojing et al., 2012), which indicates that there is a power-enhancing coupling-effect for roof-mounted turbines which is not present for ground-mounted turbine pairs. Case B is not sensitive to the relative phase angle, aligning with studies conducted on ground-mounted Savonius turbines (Xiaojing et al., 2012). Therefore, controlling the relative phase angle is not

expected to result in significant changes in performance for case B. In case C, optimal performance of $\Delta\overline{C}_{P,max} = 21.7\%$ was observed for $S = 0.2D$, similar to previous studies on ground-mounted turbine pairs (Shaheen et al., 2015; Xiaojing et al., 2012). As case C is independent of the relative phase angle, the lower power enhancement of case C is suggested to be due to a negative influence by the recirculation region. This will be further discussed in Section 3.2.2.

Figure 8 illustrates the relative performance enhancement of T1 and T2 compared to the reference case, and they are denoted as $\Delta\overline{C}_{P,T1,max}$ and $\Delta\overline{C}_{P,T2,max}$, respectively. This allows for a performance comparison between the two turbines for each configuration. It was initially expected that T1 and T2 would exhibit similar performance in cases A and B across all gap distances due to the symmetry of these configurations. However, contrary to the numerical analysis conducted by Xiaojing et al. (2012), where T1 and T2 performed equivalently in cases A and B regardless of their positions, the results of this present study revealed performance disparities between the two turbines. This difference can likely be attributed to the varying circuit resistance between T1 and T2, which ultimately leads to a generally higher performance for T2. Notably, a separate experimental study conducted by Jang et al. (2016), which investigated two Savonius wind turbines on a flat plate, also reported performance discrepancies between the turbines in counter-rotating cases.

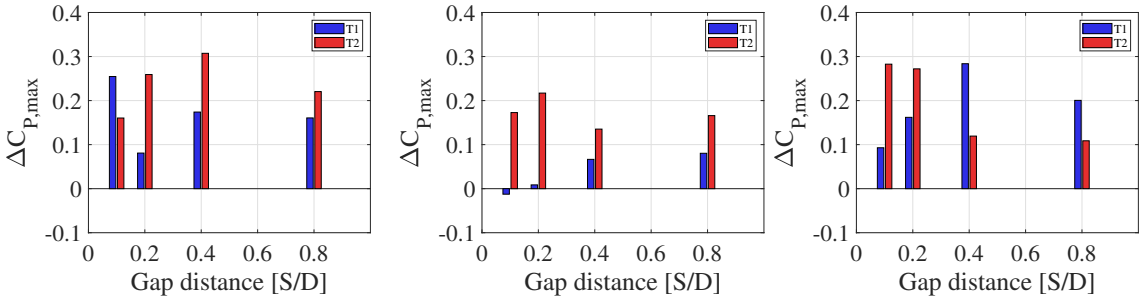

(a) Case A (b) Case B (c) Case C

Figure 8: Bar chart of the relative power coefficient for both turbines. $\Delta C_{P,max} = \frac{C_{P,max} - C_{P,Ref,max}}{C_{P,Ref,max}}$

Regarding case C, previous studies on two VAWTs mounted on a flat plate (Shaheen et al., 2015; Xiaojing et al., 2012) demonstrated that T1 outperforms T2 for all gap distances, and as the gap distance increases, the performance of T2 improves while that of T1 worsens. Interestingly, this present study observed the opposite trend. Specifically, T2 outperformed T1 for $S = 0.1D$ and $S = 0.2D$, while T1 outperformed T2 for $S = 0.4D$ and $S = 0.8D$. Furthermore, the performance of T1 increased with larger gap distances until $S = 0.4D$, whereas the performance of T2 decreased with increasing gap distances. The average performance of the turbines coincides with the findings of previous studies, although there is a slight difference in resistance for T1 and T2, as explained in Section 2.3. It is important to note that the previous studies investigated turbines on a flat plate, whereas the experiment in this present study involved roof-mounted turbines. This distinction and its possible influence will be further elaborated upon in Section 3.2.

In summary, this section emphasizes the similarities and differences of ground-mounted and roof-mounted turbine pairs regarding the existence of a coupling effect and its reliance on the relative rotational direction and gap distance. Additionally, it presents and discusses the power enhancement for roof-mounted Savonius wind turbines.

3.2. Flow Field

3.2.1. Upstream flow field

As detailed in Section 2.4, the particle image velocimetry (PIV) technique was employed to acquire flow field measurements in order to investigate the correlation between flow phenomena and the coupling effect for a turbine pair. The measurements were collected for all 12 configurations, a single roof-mounted wind turbine, and the empty roof of the model building. Additionally, the flow field was acquired for a counter-clockwise co-rotating turbine pair, case D, which is presented in Appendix B. The obtained velocity fields were time-averaged and normalized by the free stream velocity U_∞. Figure 9 displays the normalized velocity fields U/U_∞, where U is the local streamwise velocity, for the empty building and a single roof-mounted turbine, with a colorbar indicating the magnitude of velocity. As mentioned in Section 2.4, a pre-processing step involved applying a mask to the data, which is represented by the black area. The dashed line in the figures represents the leading edge of the model building. As depicted in Figure 9a, the flow field exhibits relatively uniform behavior in the y-direction, verifying that the experiments were conducted with uniform U with respect to the spanwise direction. It is observed that $U/U_\infty < 1$ due to the blockage of the rib. The velocity increases to $0.85U_\infty$ close to the building due to the accelerated flow region above the recirculation area. The favorable accelerated flow in this region results in increased performance of the turbines compared to ground-mounted turbines (Jooss et al., 2022a). Conversely, Figure 9b reveals a noticeable decrease in U/U_∞ immediately upstream of the turbine, illustrating the occurrence of a blockage effect that propagates upstream.

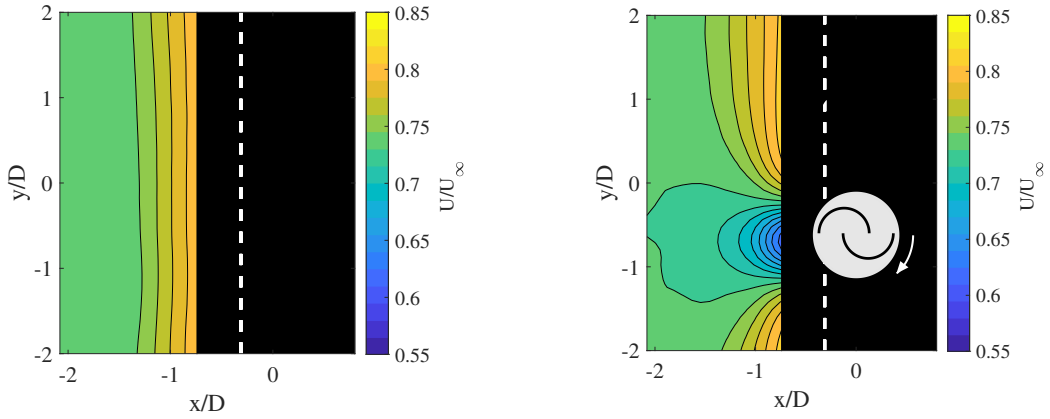

(a) Building without turbines

(b) A single roof-mounted turbine

Figure 9: Time-averaged flow field of streamwise velocity U. The masked area is depicted in black, while the leading edge of the building is represented by a dashed white line.

Figure 10 presents similar velocity plots for the turbine pair configurations, clearly demonstrating increased blockage when two turbines are present compared to a single turbine. Moreover, there is a general trend of enhanced blockage at smaller gap distances across all rotational cases. This trend can be linked to the behavior of side-by-side cylinders, where the cylinder pair behaves more similarly to a single bluff body when the gap distance is smaller (Sumner, 2010). Notably, the velocity at the centerline of the turbine pair, U_c, accelerates as the flow passes between the

turbines, which is consistent with Xiaojing et al. (2012) findings at $S = 0.2D$. Across all rotational cases, there is a noticeable decrease in U_c as the gap distance decreases, likely due to the increased effective blockage, which diverts more of the flow around the turbines.

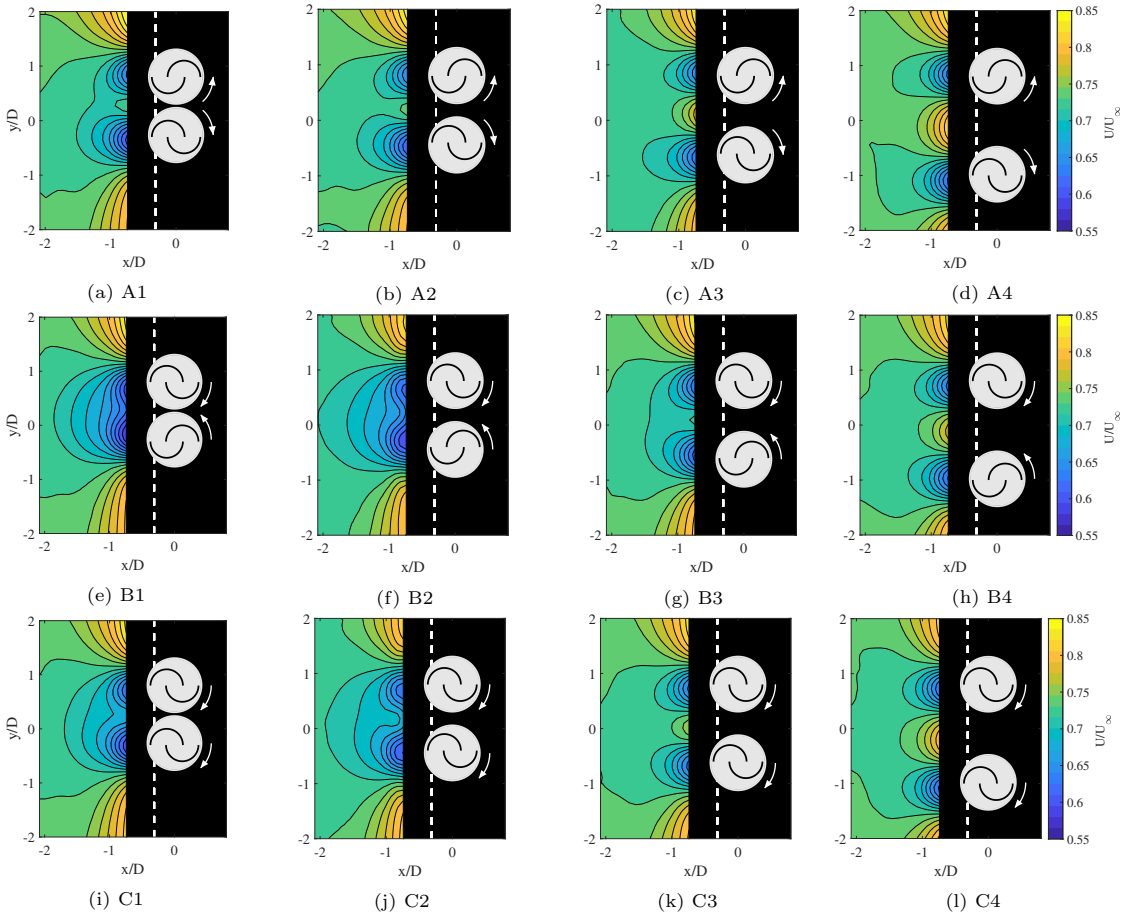

Figure 10: Time-averaged flow field of streamwise velocity U for all configurations, operating at the optimal λ for each configuration. The masked area is depicted in black, while the leading edge of the building is represented by a dashed white line.

Table 2 presents the relative change in average streamwise velocity upstream, $\overline{U}_{us}$, with respect to the average streamwise velocity upstream of the empty building, $\overline{U}_{us,b}$. The configurations A3 and C2 exhibit the highest $\overline{U}_{us}$ values for their respective cases, which aligns with their optimal gap distances in cases A and C, suggesting a potential association between higher $\overline{U}_{us}$ and improved performance for the same rotational case. Conversely, for case B, the best configuration (B4) corresponds to the lowest $\overline{U}_{us}$, indicating a possible inverse relationship in this case. These findings are indicative of a coupling effect between the turbines in case B that results in reduced negative torque, thus providing an explanation for the power enhancement. However, when examining the relationship between turbine performance and $\overline{U}_{us}$ for other configurations, inconsistent findings emerge when relating $\overline{U}_{us,b}$ to the turbine's performance. This can be attributed to the

limited field of view (FOV) insufficiently encapsulating the upstream flow field. It is hypothesized that conducting further investigations with a larger FOV for the PIV measurements would provide a better understanding of this relationship, thus motivating future research in this direction.

Table 2: Relative change in the mean upstream flow field ($\overline{U}_{us}$) with respect to the empty building case, $\frac{\overline{U}_{us,b}-\overline{U}_{us}}{\overline{U}_{us,b}}$,.

	P1	**P2**	**P3**	**P4**
A	2.7%	2.8%	3.4%	2.3%
B	3.8%	4.4%	2.9%	2.8%
C	3.3%	4.2%	2.7%	2.9%

To explore the flow behavior upstream of the turbines, spanwise line plots of normalized velocity (U/U_∞) were generated at a position $0.74D$ upstream of the turbine center for various gap distances and rotational cases. These line plots, depicted in Figure 11, illustrate the velocity deficits corresponding to the blockage effects of each turbine. U_c is lower for smaller gap distances due to the increase in effective blockage. The acceleration of the centerline velocity (U_c) follows a consistent pattern across all gap distances, with configurations A, C, and B demonstrating the highest U_c values in that order. Furthermore, the performance order of the turbine pair aligns with this pattern for the same gap distance, except for the configuration C2, which exhibits a higher $\overline{C}_{P,max}$ than A2.

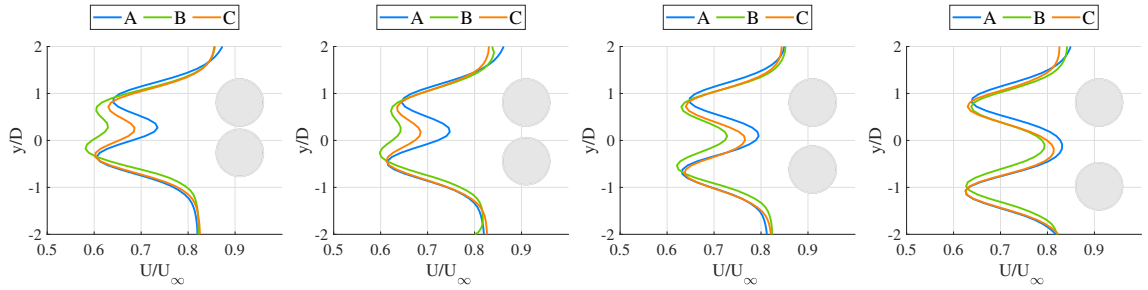

(a) $S/D = 0.1$ (b) $S/D = 0.2$ (c) $S/D = 0.4$ (d) $S/D = 0.8$

Figure 11: Time-averaged U line plots upstream of turbines.

For small gap distances, the centerline velocity changes notably between the different cases, while the difference in U_c is less prominent for larger gap distances. Between case A and B, the difference in centerline velocity $(\Delta U_c/U_\infty)_{A,B}$ is 0.106, 0.105, 0.067, and 0.038 for the gap distances 0.1D, 0.2D, 0.4D, and 0.8D, respectively. There is a 63.2% difference between the smallest and largest gap distance for $(\Delta U_c/U_\infty)_{A,B}$. This shows that the coupling effect is influencing U_c in favor of the inner buckets with regard to performance. Specifically, the coupling effect is more pronounced at smaller gap distances, resulting in a greater increase in the relative velocity (U_c) between the turbines for case A and a comparatively smaller increase for case B. This discrepancy in the coupling effect leads to a significant torque generation in the rotational direction for case A and a reduced negative torque for case B. In a study conducted by Xiaojing et al. (2012), it was found that turbines in case A efficiently redirect the accelerated centerline velocity by diverting the flow from one turbine's advancing bucket to the other turbine's advancing bucket. This correlates

with the relatively high U_c values observed for case A across all gap distances. In case B, the inner buckets are in a returning state, and the coupling effect between the turbines assists the buckets in moving against the accelerated center velocity, thus reducing the anti-rotation torque and enhancing performance. The coupling effect in rotational case C is described as a reduction in anti-rotation torque on T1, as high velocity flow is deflected from T2's returning bucket towards the advancing bucket of T1 (Shaheen et al., 2015), therefore a higher U_c would contribute to greater performance improvement for a given gap distance. These findings imply a possible correlation between the upstream flow field and the performance of the turbine.

3.2.2. Downstream flow field

In addition to examining the flow field upstream of the model building, the flow field downstream of the building was also obtained using PIV, as described in Section 2.4. Figure 12 and Figure 13 illustrate the time-averaged vorticity of the entire flow field and in the downstream region, respectively. This is an interesting parameter for this area since the coupling effect between the two turbines is closely related to vortex shedding and cyclic pressure fluctuations (Zhou et al., 2013). Analyzing the wake of the two Savonius turbines may therefore provide further insights into the coupling effect exhibited by the turbines in each configuration. Vortex shedding is expected for two ground-mounted Savonius turbines, as shown in Laws (2022). The vortices travel in the streamwise direction before they are gradually broken down and diffused by the flow as the wake recovers. Similar vortex shedding is observed in Figure 12, which presents an instantaneous and time average flow field around a single turbine in the freestream. A von Kármán vortex street is present in both figures. Due to the absence of a building, there is no recirculation area and the wake of the turbine remains undisturbed.

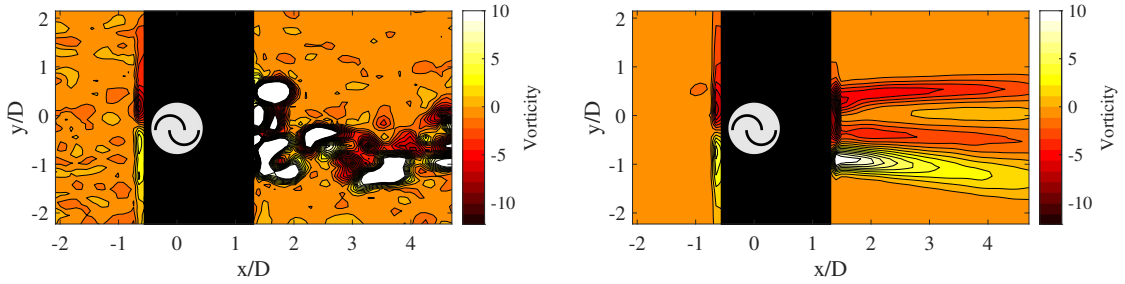

(a) Instantaneous flow field

(b) Time averaged flow field

Figure 12: The vorticity of a single turbine in freestream.

However, the vortical structures in the wake of roof-mounted turbines are subject to reversed flow inside the recirculation region. Therefore, only low-intensity vortices are present in the region behind the turbine pairs, as illustrated by Figure 13. A notable observation from the comparison

of Figure 13 and Figure 12 is the substantial reduction in vorticity, both in terms of intensity and vortex shedding pattern, caused by the recirculation region. The wake of a turbine on a flat plate is more predictable than the wake behind roof-mounted turbines, which is rapidly diffused in the recirculation region.

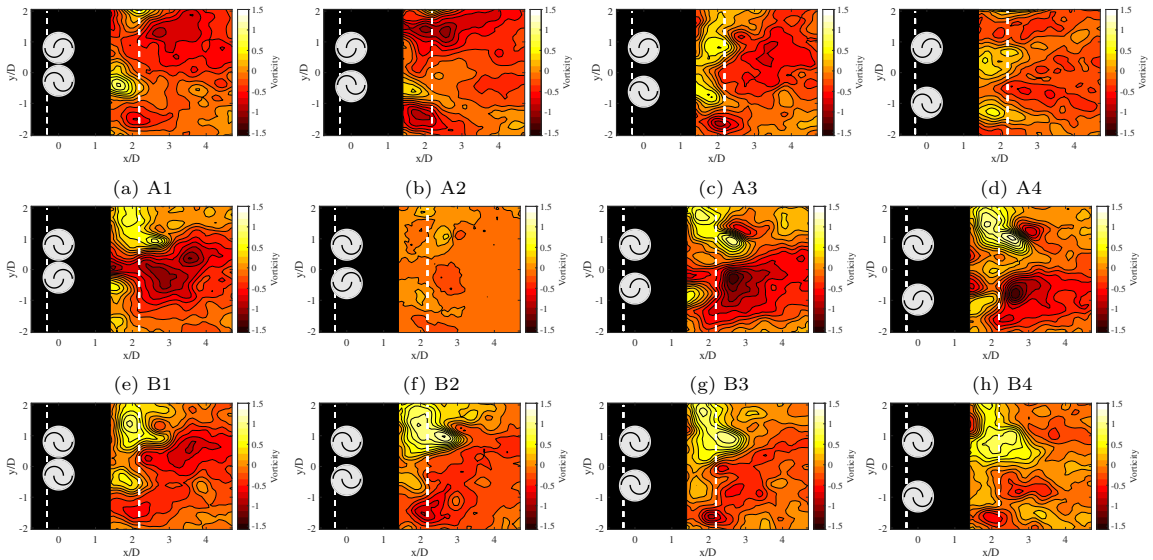

(a) A1 (b) A2 (c) A3 (d) A4

(e) B1 (f) B2 (g) B3 (h) B4

(i) C1 (j) C2 (k) C3 (l) C4

Figure 13: Time-averaged vorticity downstream of turbines.

In addition to the coupling effect between two co-rotating turbines described in Section 3.1, the vortex structures in the wake can influence the performance of the turbines. Studies have shown that suppression of vortices in the wake of a bluff body can lead to a decrease in drag acting on the object (Rashidi et al., 2016). As the Savonious turbine is drag-driven, it is reasonable to assume that the suppression of vortices caused by the influence of the recirculation region can affect the turbines' performance. For all the cases, it can be observed from Figure Figure 13 that the downstream flow field has no significant changes in characteristics and and intensity with varying gap distance. This provides an explanation for the relatively low gap distance dependence of the turbine pair, as stated in Section 3.1.

Case B generally shows greater vorticity intensity and performs worse compared to the other rotational cases. The placement of the vortices results in a lower pressure distribution behind the returning buckets, consequently resulting in increased anti-rotational torque for case B compared to the other rotational cases. However, the suppression of the downstream vortices will reduce the anti-rotational torque when compared to ground-mounted turbines that are not influenced by a recirculation region, thus providing an explanation for the overall power enhancement of case B, as described in Section 3.1. Interestingly, the result of B2 shows very low vorticity and the flow field deviates from the other cases with regard to vortices and intensity. It is contemplated that the specific configuration and λ of the two turbines shed vortices that suppress each other, similar to findings of vortex suppression for rotating cylinder pairs in parallel (Chan et al., 2011). Furthermore, since the vortex intensity of turbines is significantly reduced by the recirculation

region, large differences in performance were not found compared to the other gap distances.

For case C, the performance of T1 and T2 show an opposite trend in power enhancement when varying the gap distance compared to previous research of ground-mounted turbines, as stated in Section 3.1 and visualized in Figure 8. This difference in relation could potentially be a result of the difference in wake characteristics. The skewed flow of co-rotating turbines on a flat plate due to rotation of the turbines, i.e., the Magnus effect (Shigetomi et al., 2011), seems to be absent in Figure 13. A difference in the wake direction will influence the performance of the turbines due to changes in the downstream pressure distribution. This provides an explanation for the differing results of T1 and T2 compared to a ground-mounted turbine pair for case C. Understanding the vortex structures formed in the wake of the turbines, which induce drag, is crucial since Savonius turbines operate based on drag forces. Further research investigating the wake of ground-mounted Savonious wind turbine pairs would provide valuable insight into the relation between turbine performance and downstream wake characteristics.

4. Conclusion

This study examined the interaction between two roof-mounted Savonius turbines placed parallel to the cross-flow. Through a wind tunnel experiment, the investigation focused on analyzing the power performance of the turbines in relation to their rotational direction and the gap distance between them. The experimental setup involved acquiring power curves by measuring the power output for various tip-speed ratios, along with utilizing particle image velocimetry (PIV) to visualize the flow field. The results demonstrated that at higher tip speed ratios (λ), all configurations exhibited power enhancement compared to the reference case of a single roof-mounted turbine, due to a coupling effect between the turbine pair. Conversely, no power enhancement was observed at lower tip speed ratios, suggesting that a minimum λ is required to achieve power enhancement for the turbine pair.

The study further revealed that counter-rotating turbines with the advancing buckets placed in the gap between the rotors (case A) exhibited the most significant power enhancement across various gap distances, while counter-rotating turbines with the returning buckets placed in the gap between the rotors (case B) exhibited the lowest power-enhancing effect. Interestingly, the average power enhancement of the turbines in case B is not present for ground-mounted turbines (Xiaojing et al., 2012). Co-rotating turbines (Case C) generally displayed slightly lower power enhancement compared to case A. The optimal configuration was determined to be case A with a gap distance (S) of 0.4 turbine diameters (D). In this configuration, the average power coefficient of both turbines was found to be 24.1% higher compared to a single roof-mounted turbine. These findings align with previous numerical studies investigating the coupling effect between two turbines mounted on a flat plate (Shaheen et al., 2015; Xiaojing et al., 2012).

Furthermore, variations in power enhancement between the left (T1) and right (T2) turbines (when looking downstream) were observed for the symmetrical rotational cases. These differences were attributed to slight variances in circuit resistance, leading to a discrepancy in tip-speed ratios between the turbines. Interestingly, for the co-rotating case, the performance of T1 and T2 in relation to the gap distance diverged from previous findings on ground-mounted turbines (Shaheen et al., 2015; Xiaojing et al., 2012). It was discovered that T2 outperformed T1 for smaller gap distances, while the opposite trend was observed for greater gap distances.

Analysis of the upstream flow field indicated that the best-performing gap distance for cases A and C correlated with the highest average upstream velocities, whereas for case B, the greatest per-

formance aligned with the lowest upstream velocities. Additionally, a comparison of the centerline velocity for each configuration revealed that case A and B exhibited the highest and lowest velocities, respectively, suggesting a potential relationship between the upstream flow field and turbine performance. However, a more comprehensive investigation with a wider field of view is necessary to establish a clearer trend.

Furthermore, examination of the downstream vorticity flow field revealed that the recirculation region above the roof of the building significantly influenced the wake characteristics of the turbine pair. The presence of turbulence and backflow within the recirculation region suppressed the vortices shed from the turbine pair, resulting in the presence of low-intensity vortices. Given that vortices induce drag and Savonius turbines are drag-driven, it is plausible that the suppression of vortices impacts the turbine's performance, providing an explanation for the differing results observed in case C, as mentioned earlier. This also provides an explanation for the observed power enhancement in case B. The analysis of the downstream flow field revealed that the distribution of vortices primarily occurs behind the returning buckets of the turbines. Consequently, the presence of the recirculation region leads to the suppression of vortices, resulting in a reduction of the anti-rotational torque. Therefore, the suppression of vortices contributes to an enhancement in turbine performance for case B. Consequently, further research investigating the performance of turbine pairs in relation to downstream vortices, both for ground- and roof-mounted configurations, is of interest.

To conclude, the optimal configuration for the arrangement of two parallel roof-mounted Savonius turbines placed parallel to the cross-flow is case A, with a gap distance of 0.4D. This research has shed light on intriguing similarities between ground-mounted and roof-mounted turbines. Moreover, these findings create opportunities for further investigation, leading to a multitude of interesting questions to be explored in future research.

References

Akwa, J. V., Vielmo, H. A., & Petry, A. P. (2012). A review on the performance of savonius wind turbines. *Renewable and sustainable energy reviews*, *16*(5), 3054–3064.

Aliferis, A. D., Jessen, M. S., Bracchi, T., & Hearst, R. J. (2019). Performance and wake of a savonius vertical-axis wind turbine under different incoming conditions. *Wind Energy*, *22*(9), 1260–1273.

Arendt, S. (1993). Vorticity in stratified fluids. i. general formulation. *Geophysical & Astrophysical Fluid Dynamics*, *68*(1-4), 59–83.

Chan, A. S., Dewey, P. A., Jameson, A., Liang, C., & Smits, A. J. (2011). Vortex suppression and drag reduction in the wake of counter-rotating cylinders. *Journal of Fluid Mechanics*, *679*, 343–382.

Dabiri, J. O. (2011). Potential order-of-magnitude enhancement of wind farm power density via counter-rotating vertical-axis wind turbine arrays. *Journal of renewable and sustainable energy*, *3*(4), 043104.

Hesami, A., Nikseresht, A. H., & Mohamed, M. H. (2022). Feasibility study of twin-rotor savonius wind turbine incorporated with a wind-lens. *Ocean Engineering*, *247*, 110654.

International Energy Agency. (2022). *Energy statistics data browser*.

Jang, C.-M., Kim, Y.-G., Kang, S.-K., & Lee, J.-H. (2016). An experiment for the effects of the distance and rotational direction of two neighboring vertical savonius blades. *International Journal of Energy Research*, *40*(5), 632–638.

Jooss, Y., Bolis, R., Bracchi, T., & Hearst, R. J. (2022a). Flow field and performance of a vertical-axis wind turbine on model buildings. *Flow*, *2*.

Jooss, Y., Rønning, E. B., Hearst, R. J., & Bracchi, T. (2022b). Influence of position and wind direction on the performance of a roof mounted vertical axis wind turbine. *Journal of Wind Engineering and Industrial Aerodynamics*, *230*, 105177.

Laws, P. (2022). Validating the ideal configuration and mutual coupling effect among savonius wind turbine clusters using free rotation analysis. *Ocean Engineering*, *266*, 112879.

Mertens, S. (2003). The energy yield of roof mounted wind turbines. *Wind engineering*, *27*(6), 507–518.

Pagnini, L. C., Burlando, M., & Repetto, M. P. (2015). Experimental power curve of small-size wind turbines in turbulent urban environment. *Applied Energy*, *154*, 112–121.

Rashidi, S., Hayatdavoodi, M., & Esfahani, J. A. (2016). Vortex shedding suppression and wake control: A review. *Ocean Engineering*, *126*, 57–80.

Rønning, E. B. (2011). Influence of site, turbine height and wind direction on the performance of vertical-axis wind turbines on model buildings. *Master's Thesis*.

Roser, M., Ritchie, H., Ortiz-Ospina, E., & Rodés-Guirao, L. (2013). World population growth [https://ourworldindata.org/world-population-growth]. *Our World in Data*.

Shah, M. K., & Tachie, M. F. (2009). Piv investigation of flow over a transverse square rib in pressure gradients. *Journal of Turbulence*, (10), N39.

Shaheen, M., El-Sayed, M., & Abdallah, S. (2015). Numerical study of two-bucket savonius wind turbine cluster. *Journal of Wind Engineering and Industrial Aerodynamics*, *137*, 78–89.

Shannon, C. E. (1949). Communication in the presence of noise. *Proceedings of the IRE*, *37*(1), 10–21.

Shigetomi, A., Murai, Y., Tasaka, Y., & Takeda, Y. (2011). Interactive flow field around two savonius turbines. *Renewable energy*, *36*(2), 536–545.

Sumner, D. (2010). Two circular cylinders in cross-flow: A review. *Journal of fluids and structures*, *26*(6), 849–899.

Toja-Silva, F., Peralta, C., Lopez-Garcia, O., Navarro, J., & Cruz, I. (2015). On roof geometry for urban wind energy exploitation in high-rise buildings. *Computation*, *3*(2), 299–325.

Wheeler, A. J., Ganji, A. R., Krishnan, V. V., & Thurow, B. S. (2010). *Introduction to engineering experimentation* (Vol. 480). Pearson London, UK.

Xiaojing, S., Daihai, L., Diangui, H., & Guoqing, W. (2012). Numerical study on coupling effects among multiple savonius turbines. *Journal of Renewable and Sustainable Energy*, *4*(5), 053107.

Zhou, T., & Rempfer, D. (2013). Numerical study of detailed flow field and performance of savonius wind turbines. *Renewable energy*, *51*, 373–381.

Appendix A. Additional Results

Appendix A.1. GUNT Wind Tunnel Experiments

Two turbines, T1 and T2, were used in this experiment. Each turbine was connected to an individual electronic setup consisting of identical components. These setups enabled power measurements to be obtained for each turbine. However, a discrepancy was observed in the C_P-curves when sampling with the different setups. Despite the components being identical, a minor disparity in the switching frequency of the variable switches was observed, likely due to production uncertainties. This discrepancy resulted in a lower resistance in the circuit for T2 compared to T1 for the same k-value, which was defined in Section 2.2. This impacted the measured values for angular velocity (ω) and current (I), which were used to calculate the C_P-curve. To examine the impact of this electronic variation, a series of experiments were conducted in an open wind tunnel with a cross-sectional area of $0.292m^2 \times 0.292m^2$ produced by Gunt Hamburg.

Firstly, a no-load test (i.e., no motor resistance) was conducted for configuration A3 and the results showed that both turbines measured approximately the same rotational velocity, with a slight difference of 0.04%. This was expected since the rotational velocity of the two turbines should be approximately the same for symmetrical rotational cases (case A and B)(Xiaojing et al., 2012). Then, load was applied and the results demonstrated an increased disparity in the rotational velocities between the two turbines. Analyzing the data obtained from this load test revealed differing C_p-curves for the two turbines which indicated an inconsistency between the two circuits. As stated in Section 2.2, the variable switches play a role in controlling the λ of the turbines by altering the resistance within the circuits. Consequently, the findings from both the no-load and load tests suggest that the discrepancy in C_P between T1 and T2 for all configurations should partly be attributed to the discrepancy between the electronic setups, and specifically the circuit resistances.

To address this disparity, one proposal was to make adjustments to the power curve of turbine 2 by rectifying the rotational velocity output file, specifically by correcting the variable switch output. The corrected values would then be utilized to calculate a new C_P-curve. However, it is important to note that these corrections would be implemented after the measurements were taken. Consequently, the rotational velocity would still be inaccurately represented during the measurement process due to the discrepancy in the variable switches which could potentially impact the interaction between the turbines. To investigate this concern, the effect of increasing the tip-speed ratio (λ) of T2 on the power coefficient (C_P) of T1 was examined for all rotational cases at $S/D = 0.4$. Initially, both turbines had approximately the same λ, and then the electrical resistance of T2 was lowered to increase λ. It was observed that increasing λ for T2 resulted in a difference in C_P of T1 for all configurations. For configuration A3, B3, and C3, the relative change in C_P for T1 was -1.1%, $+4.7\%$, and -0.1%, respectively. Hence, it was concluded that adjusting the power curves of turbine 2 solely based on the difference in resistance would be insufficient, considering the influence of the turbines on each other. Therefore, the power curves were left uncorrected in this present study and the correctional efforts and reasons for the difference in power curves for symmetrical rotational cases have been explained.

Lastly, a reference curve was measured using one of the electrical setups before the difference in electrical setup was discovered. Therefore, an experiment was conducted to check if the reference curve could be used for both T1 and T2. The difference between I and ω for the two electrical setups at each measured point in the reference curve was measured. The results of this experiment are presented in Figure A.14. It can be observed that each point measured with the electronics

of T1 is slightly shifted along the curve when measured with the electronics of T2. However, the shape of the power curves remains identical. Therefore, it was concluded that it is sufficient to use the same reference curve for comparison with the power curves of both T1 and T2.

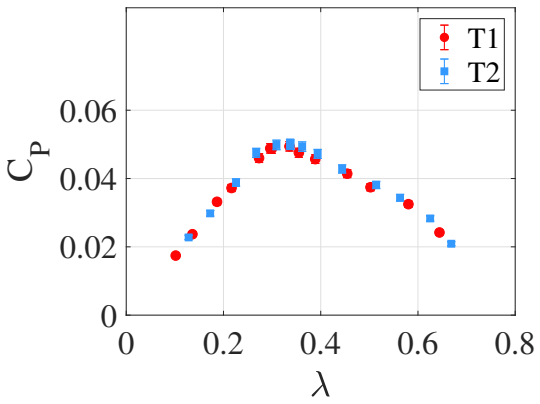

Figure A.14: A comparison between the power curves measured with the electrical setup of T1 and T2 in the Gunt wind tunnel.

Appendix A.2. Flow Fields

In case C, the turbines caused a shadow to fall on one side of the field of view (FOV) during the acquisition of PIV data. As a result, the flow field information in that particular area was lost. To address this limitation, an alternative scenario, referred to as case D, was introduced where the turbines rotated in the opposite direction compared to case C. In case D, the turbines co-rotated counter-clockwise, causing the shadow to be cast on the opposite side of the FOV. Initially, this adjustment allowed for the examination of the flow field on both sides of the turbines. However, the laser light reflected off the model turbines and disturbed the images. Therefore, the affected region had to be masked and the additional information became unavailable. Nevertheless, the flow field for case D is provided in this section as it demonstrates the anticipated similarities and differences between case C and D. The wake of case C (Figure 13i - Figure 13l) is characterized by positive vorticity, while the wake of case D is dominated by negative vorticity. This is due to the mirrored rotational direction between the cases and is a testament to the validity of the measurements. To overcome the problem due to reflections in the future, potential solutions could involve spray painting the turbines with matte black paint to eliminate the reflective surface or fabricating the turbines using a matte material. These measures could remove the reflections and enhance the quality of the captured images.

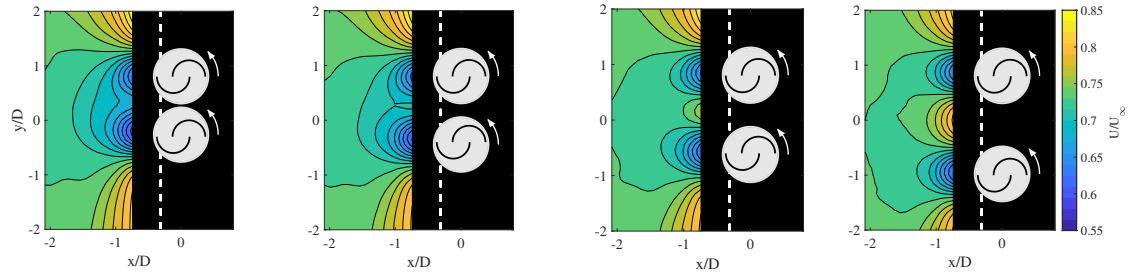

(a) D1 (b) D2 (c) D3 (d) D4

Figure A.15: Time-averaged flow field of streamwise velocity U for all configurations, operating at the optimal λ for each configuration. The masked area is depicted in black, while the leading edge of the building is represented by a dashed white line.

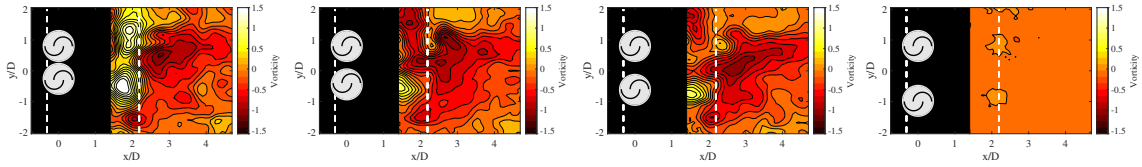

(a) A1 (b) A2 (c) A3 (d) A4

Figure A.16: Time-averaged vorticity downstream of turbines.

Appendix B. Uncertainty Analysis

To calculate the uncertainties of the measured power coefficient (C_P) and tip-speed ratio (λ), a procedure based on Wheeler et al. (2010) was employed. This method follows the law of error propagation, where the total uncertainty (σ_R) of a value (R) is determined by considering the total uncertainties (σ_n) of the input variables (x_n). The equation for calculating the total uncertainty is given by:

$$\frac{\sigma_R}{R} = \sqrt{(a\frac{\sigma_1}{x_1})^2 + (b\frac{\sigma_2}{x_2})^2 + ... + (N\frac{\sigma_n}{x_n})^2} \tag{B.1}$$

In this equation, $a, b, ..., N$ represent the exponential factors of the input variables and $\frac{\sigma_n}{x_n}$ is the relative error that includes both random and biased errors associated with x_n. The relevant input variables, along with their corresponding random and biased errors, are presented in Table B.3. The biased error of the precision manometer (FCO560) connected to the pitot was also included in the table. To estimate the random error of the current and rotational velocity, a long sample with a duration five times longer than the selected sampling time was acquired. By comparing the results obtained from the sampling time with those obtained from the long sample, the random error was determined. Other random and biased errors were found to be negligible (Rønning, 2011) and were not included in the analysis. The calculations resulted in an error of 2.80% and 1.34% for C_P and λ, respectively.

Input variable	**Measurement instrument**	**Random Error**	**Biased Error**
Freestream velocity	Pitot + FCO560	-	0.0060
Temperature	K type Thermocouple	-	0.0075
Atmospheric pressure	Mercury barometer	-	0.0001
Current	INA219 current sensor	0.0113	0.0050
Rotational Velocity	Reflective object sensor	0.0080	0.0040

Table B.3: Random and biased error of each input variable when calculating C_P and λ

Furthermore, based on previous experiments conducted by (Jooss et al., 2022b; Rønning, 2011), it was discovered that the friction torque constant provided by the motor manufacturer's data sheet ($Q_f = 0.08mNm$) overestimates the actual friction. Therefore, a constant friction torque of $Q_f = 0.01mNm$ was utilized instead. It is important to note that this adjustment does not affect the observed trends in the C_P-curves.

Appendix C. Experimental Setup

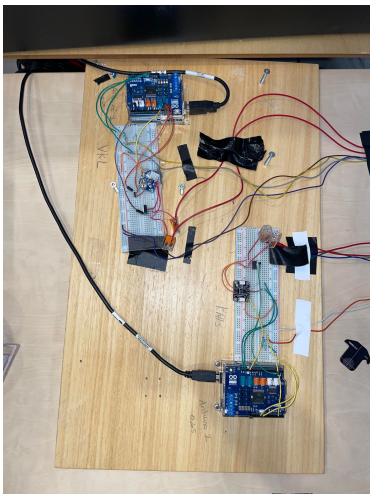

(a) The electronic setups for Turbine 1 and 2.

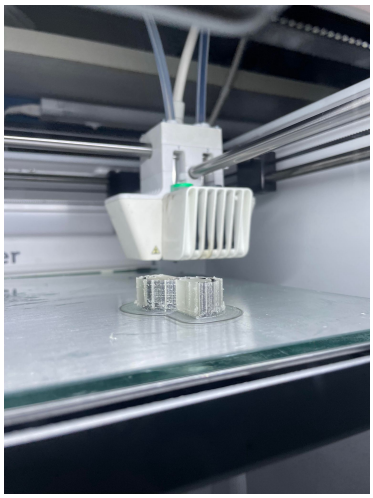

(b) Ultimaker S5 during printing of turbines.

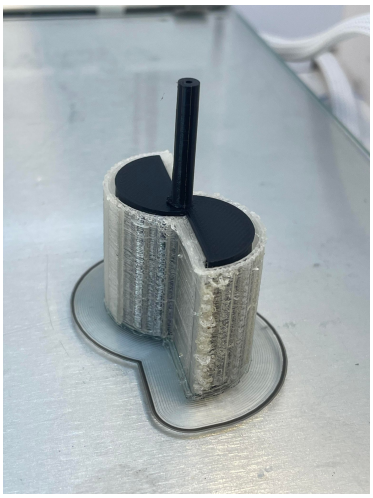

(c) A printed turbine with support structures.

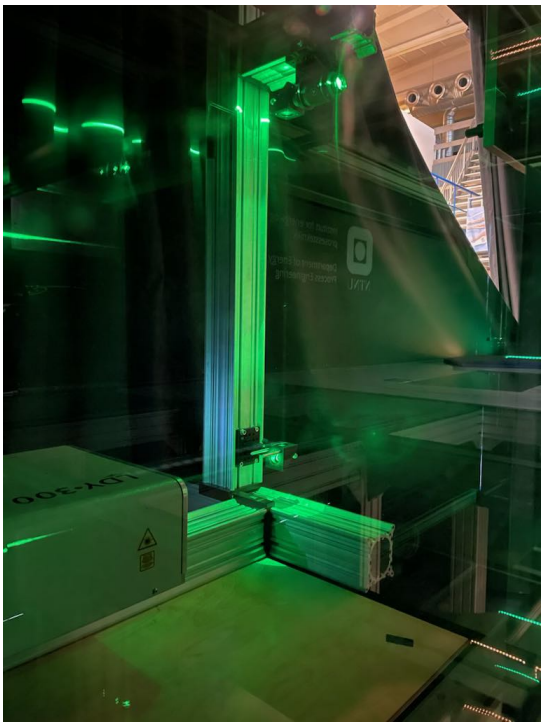

(d) Laser and optical setup for PIV.

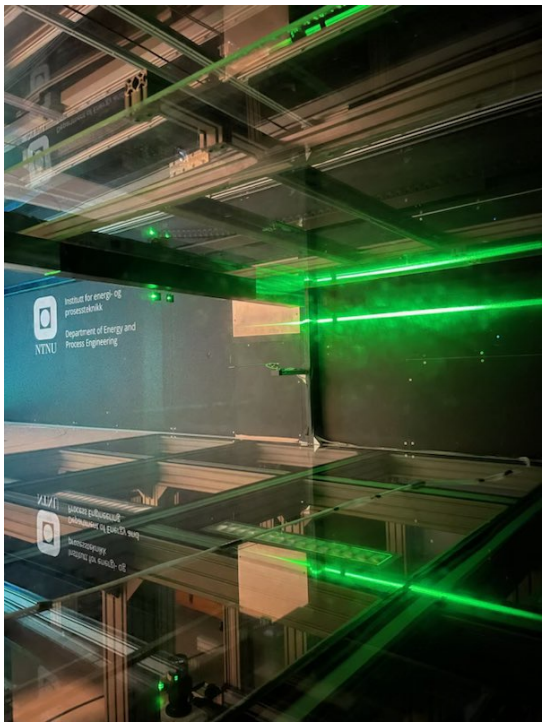

(e) Inside the wind tunnel during PIV measurements.

Figure C.17: Photos of the experimental setup.

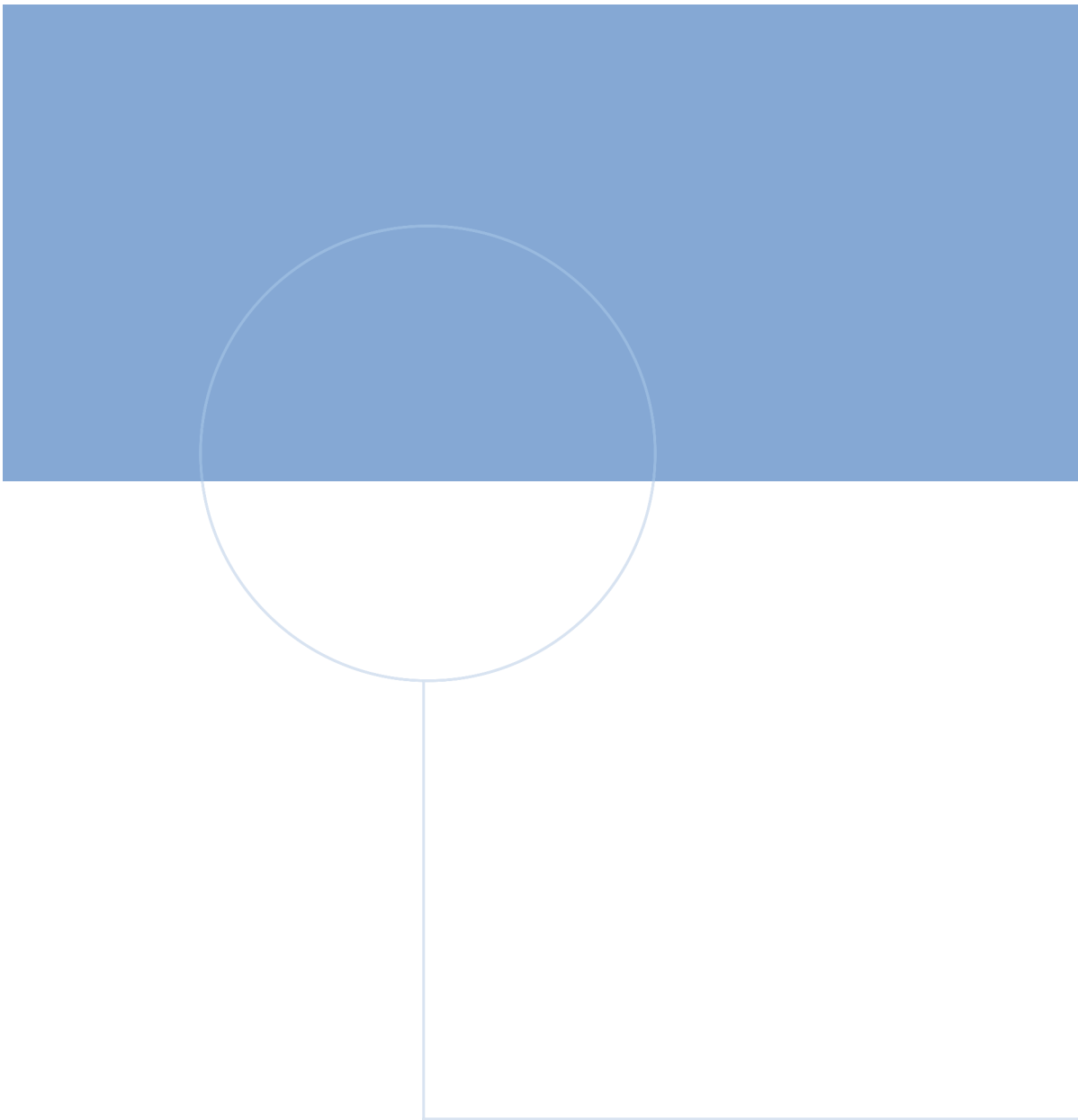

NTNU

Norwegian University of
Science and Technology